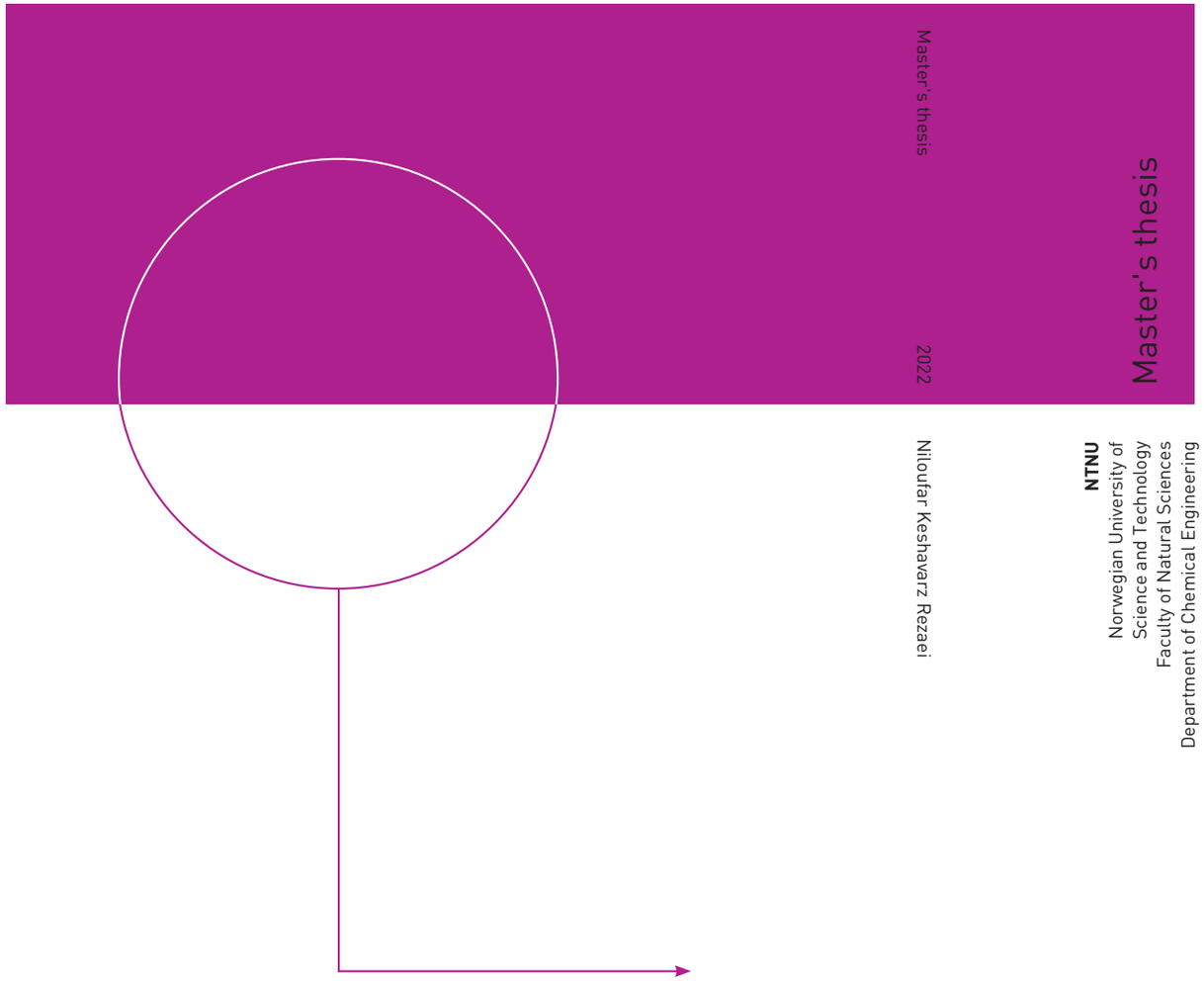

Niloufar Keshavarz Rezaei

Natural Gas Dehydration Using Membrane Contactor

July 2022

NTNU
Norwegian University of
Science and Technology

NTNU
Norwegian University of
Science and Technology

NTNU
Norwegian University of
Science and Technology

Natural Gas Dehydration Using Membrane Contactor

Niloufar Keshavarz Rezaei

Chemical Engineering
Submission date: July 2022
Supervisor: Liyuan Deng
Co-supervisor: Mahdi Ahmadi

Norwegian University of Science and Technology
Department of Chemical Engineering

NTNU
Norwegian University of
Science and Technology

Natural Gas Dehydration Using Membrane Contactor

Niloufar Keshavarz Rezaei

Chemical Engineering
Submission date: July 2022
Supervisor: Liyuan Deng, IKP
Co-supervisor: Mahdi Ahmadi, IKP

Department of Chemical Engineering
Norwegian University of Science and Technology

Preface

This master's thesis was carried out in the spring of 2022 at the Norwegian University of Science and Technology Department of Chemical Engineering. The work is a part of an ongoing PostDoc project. It is a part of a project under the administration of the Subpro group, which is a research center within the subsea processing and production field.

Foremost, I would like to express my most profound appreciation to my supervisor, Liyuan Deng, for her substantial supervision, excellent guidance and advice, and for helping me in every stage of this project. I am also thankful to my co-supervisor, PostDoc. Mahdi Ahmadi, for his outstanding support, guidance, advice, and discussion on my thesis work. Thanks to Arne Lindbråthen for his insightful comments and advice on the project and laboratory work.

I would also like to thank my parents and my brother for their love and support while I continued my studies in Norway. Last but not least, thanks to my beloved husband, Pooya. I could not have done this without his patience, support and encouragement.

" I declare that this is an independent work according to the exam regulations of the Norwegian University of Science and Technology (NTNU)."

Trondheim, 30.06.2022

Niloufar Keshavarz Rezaei

Abstract

Natural gas is the cleanest and most preferred energy source due to its high accessibility, low cost, and energy efficiency. Subsea processing aims for underwater natural gas purification at high pressures, enabling the transfer of natural gas to the market directly. It is essential to remove impurities such as water vapor, carbon dioxide, and hydrogen sulfide while operating in subsea conditions. Removing water vapor from natural gas prevents corrosion and hydrate formation in pipelines. Compared to other dehydration methods for natural gas, membrane technology has shown promising results. Membranes provide a compact design and require lower overall energy supply and cost. This project investigated the effects of operating conditions on composite membrane contactor performance in the dehydration process.

A solution of 1 wt% Teflon AF2400 in solvent FC-72 was employed to make a composite membrane on the polypropylene fibers. The thickness of the dense layer and the support pore conditions were investigated using SEM images, and a thickness of 2.77 [µm] was obtained. The selectivity of the membrane of CO_2 over N_2 was studied in a single gas permeation rig. The membrane had a selectivity of 5.3 and 5.2 at a pressure of 1 and 2 [bar], respectively. The effects of operating conditions (i.e., gas flow rate, liquid flow rate, and pressure) on membrane performance were examined. The results showed an increase in water flux while the gas flow rate and pressure increased. However, the effect of the liquid flow rate was negligible. In addition, long-term operations for 30 days were carried out, and a maximum of 10.3% decrease in gas flow rate was obtained.

Table of Contents

List of Figures **vii**

List of Tables **viii**

1 Introduction **5**

1.1 Subsea natural gas processing 5

1.2 Natural gas dehydration process 6

1.3 Natural gas dehydration using membranes 7

1.4 Thesis outline 8

2 Theory, Background and Literature Review **9**

2.1 Gas transport mechanism through membranes 9

2.2 Membrane material 12

2.3 Solvent for dehydration process 16

2.4 Membrane modules 17

2.5 Membrane contactor 19

2.5.1 Mass transfer in membrane contactors 23

3 Experiments **25**

3.1 Chemicals and materials 25

3.2 Membrane module 25

3.3 Synthesis and membrane preparation 26

3.4 Morphological characterization 28
3.5 Single gas permeation setup 28
3.6 Membrane contactor testing setup 30
3.7 Operating parameters 31
3.7.1 Liquid flow rate effect 31
3.7.2 Gas flow rate and pressure effect 32
3.8 Durability validation test 33

4 Results and Discussion **34**

4.1 Morphological characterization result 34
4.2 Gas permeation and selectivity 34
4.3 Liquid flow rate effect 35
4.4 Gas flow rate effect 37
4.5 Pressure effect 38
4.6 Validation tests results 39

5 Conclusion **41**

Bibliography **43**

List of Figures

1 Gas transport mechanisms in membranes 10

2 Gas sorption in glassy polymers based on dual-sorption model 14

3 water vapor permeability and H_2O/CH_4 selectivity in various polymers plot 15

4 Teflon AF2400 chemical structure 16

5 Plate-and-frame membrane module illustration 17

6 Spiral-wound membrane module illustration 18

7 Hollow-fiber membrane module illustration 18

8 Tubular membrane module illustration 19

9 Illustration of a membrane contactor 20

10 Pore wetting illustration 21

11 Wettability ratio impact on gas absorption flux 22

12 dense layer effect on natural gas dehydration process 23

13 concentration profile in membrane contactor 24

14 Polypropylene fiber stucture 25

15 The in-house membrane module 26

16 The procedure of sealing the module from both ends using epoxy glue 27

17 Coating 1 wt% Teflon AF2400 solution in FC-72 solvent on PP fibers 28

18 Single gas permeation setup flow diagram 29

19 The flow diagram of membrane contactor setup 31

20 SEM image of Teflon AF2400/PP composite membrane 34

21 Water flux as a function of liquid flow rate 36

22 Water flux as a function of gas flow rate 38

23 Water flux as a function of pressure 39

24 The SEM images of membrane before and after durability test 40

List of Tables

4 The prepared tubular module specifications 26

5 Data experiments for permeability tests 30

6 Effect of liquid flow rate on water flux tests 32

7 Pressure and gas flow rate effect 32

8 Randomly selected values for validation tests 33

9 Gas transport parameters of Teflon AF2400 35

10 Liquid flow rate effect on water vapor flux 35

11 The effect of gas flow rate on water vapor flux 37

12 Experimental results of the effect of pressure on water vapor flux . . . 38

13 Validation tests results: (a) denotes to tests before long-term operation, (b) denotes to tests repeated after long-term operation. 39

Nomenclature

Symbol	Description	Value/Unit

Latin letters

A_m	membrane area	cm^2
Å	the angstrom unit	10^{-10} m
P	permeability	Barrer
D	diffusivity coefficient	cm^2/s
S	solubility coefficient	$cm^3(STP)/cm^3cmHg$
J	flux	mol/m^2s
Δp	pressure difference	kPa
l	thickness	mm
T_g	glass transition temperature	°C
C_D	gas concentration by Henry's law	mol/m^3
K_D	sorption constant	-
C_H	gas concentration by Langmuir model	mol/m^3
C'_H	saturation sorption	mol/m^3
b	affinity constant	-
p	pressure	bar
$C_{g,i}$	concentrations in gas phase	mol/m^3
$C_{gm,i}$	concentrations in gas-membrane interface	mol/m^3
$C_{lm,i}$	concentrations in liquid-membrane interface	mol/m^3
$C_{l,i}$	concentrations in liquid phase	mol/m^3

K_{ov}	overall mass transfer coefficient	m/s
K_g	local mass transfer coefficient of gas phase	m/s
K_l	local mass transfer coefficient of liquid phase	m/s
K_m	mass transfer resistance in the membrane	m/s
$r_{p,max}$	maximum radius of the pores	µm, m
T	temperature	°C
dp/dt	steady-state increase in pressure	cmHg/s
V_d	downstream volume	cm^3
R	gas constant	cm^3cmHg/cm^3(STP)K
		or atm L/mol K
F_G	gas flow rate	ml/min
F_L	liquid flow rate	g/h
$y_A{}^{inlet}$	inlet water vapor mole fraction	ppmv
$y_A{}^{outlet}$	outlet water vapor mole fraction	ppmv
M_w	water molecular weight	g/mol

Greek letters

λ	mean free path	m
γ	surface tension of the liquid phase	N/m
α	selectivity	-
β	process separation factor	-
θ	contact angle between liquid and membrane	°

γ_{H_2O}	activity coefficient of water	-
φ_{H_2O}	fugacity coefficient of water	-
$p^{sat}_{H_2O}$	saturated water vapor pressure	kPa

Abbreviations

PEO-PBT	poly(ethylene oxide)-poly(butylene terephthalate)
SPAI	sulfonated poly(amide imide)
CA	cellulose acetate
BDD	2,2-bistrifluoromethyl-4,5-difluoro1,3-dioxole
TFE	tetrafluoro-ethylene
MEG	mono-ethylene glycol
TEG	tri-ethylene glycol
TREG	tetra-ethylene glycol
PP	polypropylene
PTFE	polytetrafluoroethylene
PVDF	polyvinylidene fluoride
PTMS	poly(1-trimethylsilyl-1-propyne)
PIM	Polymer of Intrinsic Microporosity
MEA	monoethanolamine
PTMSP	poly(1-trimethylsilyl-1-propyne)
DP	dew point

Chapter 1

1 Introduction

1.1 Subsea natural gas processing

Natural gas is a combination of gaseous hydrocarbons that has become a preferred fuel due to its low cost, environmental sustainability, high accessibility, and abundant reservoirs [1, 2]. It is more environmentally friendly than other fossil fuels such as coal, gasoline, and diesel, since its combustion is cleaner owing to its lower carbon content [1, 2, 3]. Moreover, compared to coal and oil combustion, natural gas combustion generates fewer nitrogen oxides (NO_x) and sulfur dioxide (SO_2). It mainly contains methane, small amounts of other hydrocarbons, hydrogen sulfide, carbon dioxide, nitrogen, and water. Components other than methane must be removed before transporting it through pipelines. Hence, lately, subsea oil and gas processing has attracted significant interest [1, 2].

Subsea processing eliminates the need for onshore natural gas purification and treatment, reduces both the capital and operating costs, boosts productivity, reduces the amount of energy supply required, and enhances overall efficiency. Furthermore, it reduces the probability of fire and explosions, which minimizes personnel health risks [4]. However, it also faces some limitations. Since it is controlled remotely, the process should have as few moving parts as possible. In addition, the process should have low regular maintenance requirements, a high degree of modularity, and high accessibility. Furthermore, subsea equipment must be small and lightweight due to crane limitations [4]. Other aspects that need to be considered include flexibility in terms of flow rate and composition, as well as operation at high pressures for more efficient use of energy [4, 5].

1.2 Natural gas dehydration process

Various purification processes are required to convert natural gas into clean, dry fuel. Prior to transferring natural gas to the market, impurities and heavy hydrocarbons must be removed. The purification processes include removing water vapor, oil, hydrogen sulfide, nitrogen, and carbon dioxide[1, 3]. The dehydration process removes water vapor from natural gas, mitigating potential risks associated with transporting natural gas upstream. While natural gas is conveyed through pipelines installed in the deep sea, at high pressure and low temperature, water vapor may induce hydrate formation and even ice in this condition, resulting in pipeline clogging and corrosion. The pipeline corrosion rate is a critical factor in the pipeline lifetime. In addition, water vapor may induce blockage in process equipment and valve fittings in the presence of CO_2 and H_2S. Hence, water vapor should be eliminated from natural gas.

The water content of natural gas can be expressed in terms of water dew point. It denotes the temperature at which natural gas is saturated with water vapor at a specific pressure. A low level of dew point is an indication of low water vapor content. Therefore, a lower dew point is desired to prevent hydrate formation and corrosion in pipelines [1, 2, 3].

Primitively, the pipelines were short. Hence, line heaters were employed to keep the gas temperature above the water dew point. However, the discovery of reservoirs far from the shore results in longer pipelines, making the traditional techniques ineffective. Adsorption, absorption, condensation, and membrane technology are various techniques that could be employed to eliminate water vapor from natural gas[2, 3]. Both absorption and adsorption remove water vapor physically at low temperatures and high pressures. In absorption, liquid desiccants like glycol are used, whereas in adsorption, solid desiccants are utilized. However, in the condensation method, the cooling gas is used to condense water vapor[3]. Adsorption and absorption are not suitable methods in subsea processing due to their low degree of modularity and complexity [4, 5]. On the other hand, membrane technology offers compact design, high flexibility, and low maintenance, making it a viable solution for the dehydration process.

1.3 Natural gas dehydration using membranes

In subsea processing, compact and lightweight equipment is preferred. In addition, the process should have low maintenance, high accessibility and flexibility. Membrane technology is a novel strategy with a number of benefits that aims to eliminate subsea processing limitations. Membranes provide compact design, less complexity and less maintenance. Easy and linear scale-up, smaller footprint and simplicity in operations are the other membrane benefits. Additionally, employing membranes reduces energy usage and operational and capital costs.

In subsea gas processing, however, selecting suitable membrane materials and modules is essential for maintaining stable conditions and reliable performance. Most reports have demonstrated high performance for polymeric membranes in water vapor removal of topside processes. However, vacuum or sweep gas on the permeate side, which provides the required driving force for the process, causes methane loss on the permeate side as well as complexity challenges for subsea processing. With a methane loss of even 1%, membrane technology loses its priority over conventional methods. The membrane contactor provides a membrane process with absorption advantages, eliminating the problem of methane loss at high pressure. This hybrid membrane combines the benefits of high modularity of membrane technology with high selectivity of the absorption process. Other benefits of membrane contactors include large interfacial areas and no flooding or foaming. It provides an interface between the two phases, resulting in no phase contact between liquid and gas. The gas phase passes through one side of a membrane contactor while liquid absorbent flows through the other side [4, 5].

1.4 Thesis outline

The overall structure of this thesis is in the form of five chapters.

***Chapter*1** provides an introduction to subsea processing and a comprehensive description of membrane usage for subsea natural gas dehydration.

***Chapter*2** presents an overview of the theory, background, and literature review of membrane technology and transport mechanisms in membranes, especially in membrane contactors. Besides, different membrane materials and modules were introduced.

***Chapter*3** represents membrane preparation and characterization procedures. Moreover, experiments to measure the fabricated membrane's selectivity and permeability, the effects of the operating conditions on water removal, and membrane performance after long-term operation were described.

***Chapter*4** provides the membrane morphological characterization results in addition to its selectivity and permeability. This chapter investigated the effects of liquid flow rate, gas flow rate, and pressure on water flux. Furthermore, the impact of long-term operation on membrane performance was examined.

***Chapter*5** explains in detail the conclusions drawn from the findings of the experiments.

Chapter 2

2 Theory, Background and Literature Review

The most widely utilized industrial gas separation process is natural gas processing [6]. Membranes have shown potential application for natural gas processing under subsea conditions. This technology offers less complexity, high modularity, and fewer moving parts. Besides, it provides lower energy consumption and costs, making membrane processes a suitable approach for subsea natural gas dehydration. However, the high pressure underwater makes this process challenging. Polymeric membranes are the most widely used membranes for natural gas purification due to their manufacturing simplicity. According to Robeson plot [7], The performance of the membrane is bounded by a trade-off relationship between permeability and selectivity. Hence, improving the polymer properties to exceed the well-known "upper bound" is essential.

Since pressure is high in pipelines under subsea conditions, water vapor present in the natural gas can lead to swollen polymeric membranes. Therefore, membranes with high mechanical and chemical stability are preferred. Moreover, preventing methane loss is crucial in order to make this process economically feasible. Methane loss of more than 1% makes this process less cost-effective.

This chapter first provides a background on different gas transport mechanisms through the membranes, following a review of polymeric materials used for natural gas processing and their usage challenges. Moreover, membrane modules are introduced. Finally, The theory and background of membrane contactor and the mass transfer mechanism are discussed with its potential application for subsea dehydration of natural gas.

2.1 Gas transport mechanism through membranes

Difference in gas permeation rates in membranes is due to the membranes' morphology and structure differences. Despite the membrane material, transport mechanisms in porous

membranes are mainly a function of the pore sizes. Knudsen diffusion, surface diffusion, capillary condensation, molecular sieving, and solution-diffusion are transport mechanisms in membranes [8, 9]. Figure 1 illustrates the transport mechanisms in membranes.

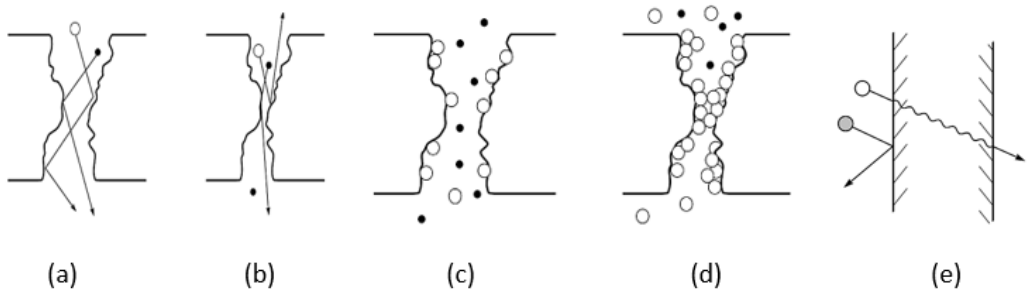

Figure 1: Gas transport mechanisms in membranes: (a) Knudsen diffusion, (b) molecular sieving, (c) Knudsen diffusion and surface diffusion, (d) surface diffusion and capillary condensation, (e) solution-diffusion in dense membranes [9]

If the pore size is more than 0.1 [μm], convective flow based on Poiseuille's law is the dominant transport mechanism in the membrane. As the pore size diameter reduces to 100-500 Å, the mean free path (λ) of gas molecules becomes bigger than the pore size. Hence, the collision between gas molecules and the pore walls is more likely. Thus, the Knudsen diffusion transport mechanism controls the penetration of gas molecules [8, 9]. As Knudsen permeability is dependent on molecular velocity, separation of molecules is based on the molecular weight ratio of gases [10].

The governing transport mechanism in membranes such as zeolites, carbon membranes, and inorganic membranes is molecular sieving. In membranes with a pore size ranging from 5-20 Å, molecular sieving is the dominant transport mechanism. In this type of membrane, the molecules with a larger mean free path than pore diameter cannot go into the membrane pores [4, 5]. Hence, selectivity in these membranes with small pores is higher than in membranes with other transport mechanisms.

In the surface diffusion mechanism, the gas molecules adsorb on the pore's surface when the pore diameter becomes less than 100 Å. These adsorbed molecules can move, and they diffuse along the membrane on the surface of the pores. Hence selectivity of the membrane is dependent on both diffusion and absorption [8, 9, 10]. Capillary condensation is when

the gas phase consists of a condensable gas, and molecules condense on the pore walls [8].

Solution-diffusion is the governed transport mechanism in nonporous membranes. Gas molecules on the feed side absorb into membrane at the gas-membrane interface and then desorb on the other side of the membrane. Gas permeation in dense membranes is dependent on two factors: solubility and diffusivity. Solubility is a thermodynamic parameter, while diffusivity is a kinetic parameter [8, 9]. Solubility is the amount of feed that adsorb by the membrane at equilibrium conditions, and it increases by growing the size of the gas molecules and critical temperature. However, diffusivity is the transportation of molecules in the membrane [8, 9]. The geometry and size of the molecules are determining factors in the diffusion of the molecules in membranes. Smaller molecules have a higher diffusion coefficient. Pressure, temperature, or concentration gradient are potential driving forces for this mechanism.

Permeability is an intrinsic property of a membrane that is affected by both solubility and diffusivity of a gas molecule and is defined by equation 1:

$$P = D \times S \tag{1}$$

The permeability coefficient, P, is membrane property that is determined by membrane material. the common unit of permeability is Barrer where 1 Barrer= 10^{-10} [cm^3 (STP).cm/ cm^2.s.cmHg]. D is diffusion coefficient [cm^2/s] and S is solubility coefficient [(cm^3 (STP)/ cm^3.cmHg)] of the gas molecules in nonporous polymeric membranes. The molar flux, J [mole/m^2s] of component i through the membrane is described as:

$$J_i = \frac{P_i}{l}\Delta p \tag{2}$$

where Δp is the partial pressure difference of component i across the membrane [kPa] and l is the thickness of the membrane [m]. Another important term in gas separation in membranes is the separation performance of membranes which is defined as the ideal selectivity of a component i compared to component j, $\alpha_{i/j}$, and is equal to the permeability of the

gas i over gas j:

$$\alpha_{i/j} = \frac{P_i}{P_j} = (\frac{D_i}{D_j})(\frac{S_i}{S_j}) \tag{3}$$

$(\frac{D_i}{D_j})$ is the diffusivity ratio of component i over j and $(\frac{S_i}{S_j})$ is the solubility ratio of component i over j. The process separation performance, which is defined as β_{ij} is another key parameter, as it shows the ability of the process to separate the desired species and is given by equation 4:

$$\beta_{ij} = \frac{y_i/y_j}{x_i/x_j} \tag{4}$$

2.2 Membrane material

An important factor in choosing membrane material is its endurance in long-term operating conditions. In gas separation processes, a membrane with high permeability and selectivity is favored [11]. Inorganic membranes have higher chemical and thermal stability than polymeric membranes; however, their high price is prohibitive [12]. Polymeric membranes are classified as glassy and rubbery membranes. Glass transition temperature (T_g) is the temperature at which the polymer state changes from glassy to rubbery. In glassy polymers where the polymer temperature is below T_g, the polymer chains are fixed and the polymer backbones cannot rotate freely. Glassy polymers have better diffusion selectivity. Therefore, small molecules are more dominant in permeating through the membrane than larger ones. Conversely, at temperatures Above T_g, The chains are flexible and the polymer has a soft and elastic form. Rubbery polymers have higher diffusion coefficients and lower solubility coefficients [13]. Despite diffusion coefficient, which is easily affected by the polymer chains and its flexibility, the sorption coefficient is dependent on condensability and molecule size of gases [8].

The dual-sorption model is used to describe solubility in polymers [8]. In rubbery polymers, gas molecules are only dissolved in the equilibrium free volume portion of the poly-

mer. Hence, the number of molecules (C_D) in this type of polymer is dependent on the pressure of the gas and is approximated by equation 5:

$$C_D = K_D.p \tag{5}$$

Where C_D is the gas concentration, K_D is the sorption constant and p is the partial pressure of the gas. The number of molecules (C_H) absorbed into the excess free volume is expressed by the Langmuir absorption equation 6:

$$C_H = \frac{C'_H bp}{1 + bp} \tag{6}$$

C'_H is the saturation sorption when all excess free volume is filled and b is the affinity constant. In glassy polymers, total sorption (C) is defined by dual-mode sorption as it is shown in equation 7, where both Henry's law and Langmuir sorption play an important role:

$$C = C_D + C_H = K_D.p + \frac{C'_H bp}{1 + bp} \tag{7}$$

Based on this model, sorption is significantly dependent on the gas pressure. As indicated in Figure 2, at low pressure, Langmuir sorption controls the gas sorption mechanism in polymers, while at high pressure, Henry's law is dominant [8].

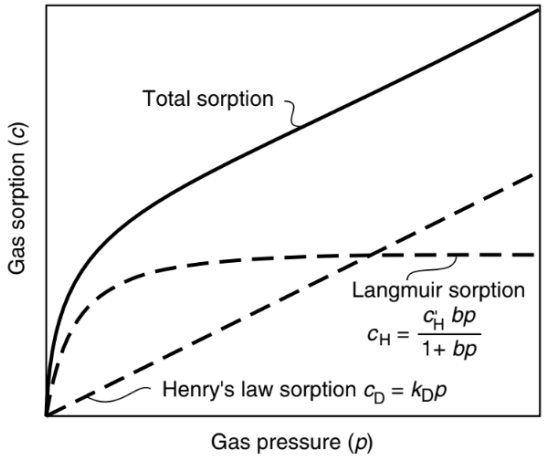

Figure 2: Gas sorption in glassy polymers based on dual-sorption model [8]

Another critical factor in choosing suitable membrane material is the presence of impurities on the feed side. Natural gas streams contain water, CO_2, H_2S and heavy hydrocarbons and aromatics, which tend to cause degradation and plasticization of membranes at high pressures. The polymer swells as a result of these impurities condensing on it, leading to selectivity reduction [6].

Among different materials, cellulose acetate and polyimides are the most frequently used membranes in industry for gas separation processes. Cellulose acetate-based membranes are the most widely used membranes for CO_2 removal, as they are considered the reference material for comparison. Despite its popularity, it plasticizes in the presence of CO_2 or other heavy hydrocarbons, reducing membrane performance and mechanical stability. Furthermore, when the feed is a mixture of gases, by increasing the pressure, the permeability of gases in the membrane decrease due to competitive sorption effects[6].

Polyimides are glassy polymers extensively used in industry with high water permeability and high CH_4 selectivity. Polyimide is a material with outstanding thermal and mechanical stability [6, 12]. The same disadvantages of cellulose acetate-based membranes are applied to polyimides. Besides, it has been demonstrated that ammonia and aromatic hydrocarbons have negative impacts on polyimides[6]. Sulfonated polymers, which are made by sulfonation of aromatic rings, are suitable for the dehydration process as well. By increasing sulfonation, water vapor permeability increases, while methane permeability

decreases. Hence, H_2O/CH_4 selectivity remarkably increases [12].

Membranes with high selectivity and permeability are preferred for natural gas dehydration. Water vapor condensability is reported to be much higher than methane. Hence water has higher solubility compared to methane. In addition, the molecular size of water is less than methane, leading to higher diffusivity. Thus, water has better permeability than methane in almost any type of polymer. Lin et al.[11], investigated the performance of various polymers reported for H_2O/CH_4 separation. They classified the polymers into four groups based on their hydrophobicity/hydrophilicity and glassy/rubbery states. Water vapor diffusivity is higher in rubbery polymers than in glassy polymers owing to the flexible chains. Moreover, hydrophobic polymers are water repulsive, which induce low water solubility than hydrophilic membranes. As shown in Figure 3, hydrophilic rubbery and glassy polymers have higher water selectivity than hydrophobic polymers. Hydrophilic rubbery polymers such as Pebax, PEO-PBT and Nafion have also shown high permeability and selectivity of water. Among hydrophilic glassy polymers, sulfonated poly(amide imide) (SPAI) and Cellulose acetate (CA) are reported to have high selectivity but lower permeability compared to rubbery polymers.

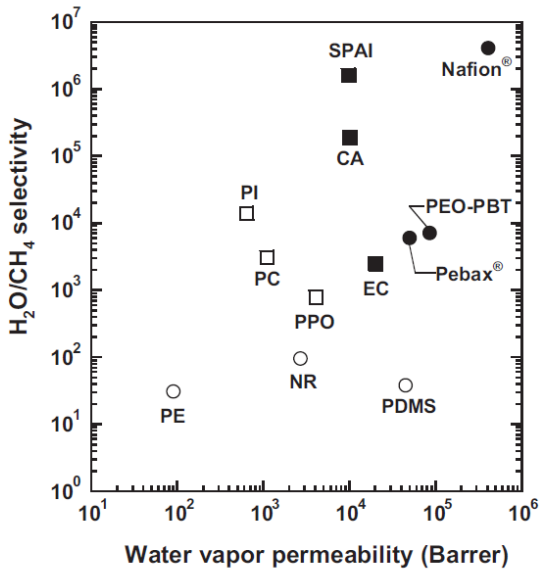

Figure 3: Comparison of water vapor permeability and H_2O/CH_4 selectivity in various polymers. [11]

Perfluoropolymers are another type of polymer that have demonstrated great chemical

and thermal stability and less susceptibility to plasticization. A high degree of crystallinity that causes low gas separation performance is the major drawback of this membrane material. However, amorphous perfluoropolymers have shown exquisite potential in gas separation [6]. Teflon AF2400 is a type of perfluoropolymers which is an amorphous glassy copolymer consists of 87 mol% 2,2-bistrifluoromethyl-4,5-difluoro1,3-dioxole (BDD) and 13 mol% tetrafluoro-ethylene (TFE). The chemical structure is shown in Figure 4. The glass transition temperature (T_G) in AF2400 is 240 °C and its density is 1.74 [gr/cm^3] [5]. Besides, it is a hydrophobic polymer with a high free volume. Jansen et al.[14] investigated the permeability of various gases in AF2400 polymer and it is reported that, the permeability of CO_2 and N_2 were 2980 and 580 [Barrer], respectively. Hence, the selectivity of CO_2 over N_2 at 25°D and pressure feed of 1 bar, was 5.1. Although the transport mechanism of water molecules in Teflon is based on solution-diffusion, it is believed that molecular sieving is the main reason for high water vapor separation performance[15]. Its high free volume, less tendency to swelling and compatibility with TEG as solvent make it a good candidate for dehydration processes[16, 17, 18].

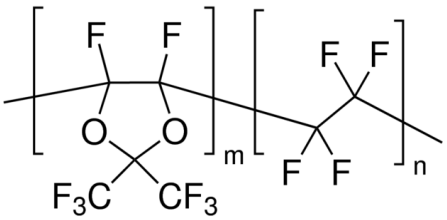

Figure 4: Teflon AF2400 chemical structure [19]

2.3 Solvent for dehydration process

Glycols are the most widely used absorbers for dehydration processes. Hydroxyl groups in glycols form hydrogen bonds which cause good performance in absorbing water. Mono-Ethylene Glycol (MEG), Di-Ethylene Glycol (DEG), Tri-Ethylene Glycol (TEG), and Tetra-Ethylene Glycol (TREG) are various types of glycol that are used in the dehydration process. Among different types of glycol, TEG is the most used absorber due to its high chemical stability, low vapor pressure, and low thermal degradation [3].

2.4 Membrane modules

A membrane provides a large surface area that is efficiently arranged and sealed in a membrane module. Effectively developed modules boost fluid hydrodynamic conditions, eliminate concentration polarization, and generally improve system operation [20, 8, 21]. In addition, the membrane module should adapt to a broad range of operating conditions. Plate-and-frame, spiral-wound, hollow-fiber and tubular are the four frequently used membrane module configurations [8, 20].

The plate-and-frame module (Figure 5) is the primary and most straightforward design. The membrane, feed spacers, and product spacers are arranged together between two end plates. This configuration which is more expensive than others is mainly used in electrodialysis and pervaporation. However, leakage through the gaskets of each plate and low packing density ($350 - 500[m^2/m^3]$) are plate-and-frame critical issues [20, 8].

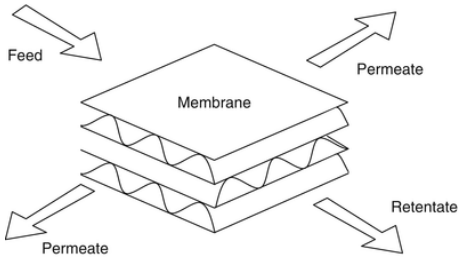

Figure 5: Plate-and-frame membrane module illustration [22]

Spiral-wound module configuration (Figure 6) is the same as plate-and-frame, where several flat-sheet membranes, feed and permeate channels, and spacers are wound around a central tube that collects permeate. The whole system is installed inside a tubular pressure vessel[23]. This module is mainly used for reverse osmosis and nano-filtration processes[24]. The feed flows in the direction parallel to the central tube in feed channels. The flow on the permeate side, which passes through the membranes, moves towards the collecting tube to leave the module. The geometry of the membranes, spacers, fouling of membranes and capability of cleaning, and operating conditions impact the performance of this configuration[23]. Spiral-wound modules have packing densities ranging from $(650 - 800[m^2/m^3])$, which is higher than plate-and-frame modules[20]. However, long permeating path and difficulty in cleaning are its main drawbacks.

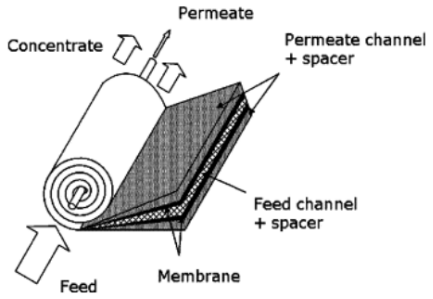

Figure 6: Spiral-wound membrane module illustration[23].

Hallow-fiber membrane modules (Figure 7) are the most extensively used configuration in the industry, which can be employed in micro/ultra/nano filtration, reverse osmosis, gas separation and pervaporation[21]. It offers higher packing density ($7000 - 13000$ $[m^2/m^3]$) for processes with footprint limitations [20]. Other major advantages of this module are higher operating flexibility, lower cost, and disposing of spacers [20, 25]. The module is separated into two parts: the shell side and the lumen side. The lumen side is the inside of the membrane fibers; however, the shell side is the space between the housing tube and the outer side of the fibers. There are two possible flow patterns in this configuration. The first flow pattern is when the feed flows in the fibers, and the permeate is in the shell side. In the second option, the feed passes through the shell side and the permeate is diffused and collected on the lumen side. Controlling flows play an important role in hollow-fiber membrane contactors[20]. Although this configuration benefits from high surface area per unit volume, high pressure drop and laminar flow are its main drawbacks[22].

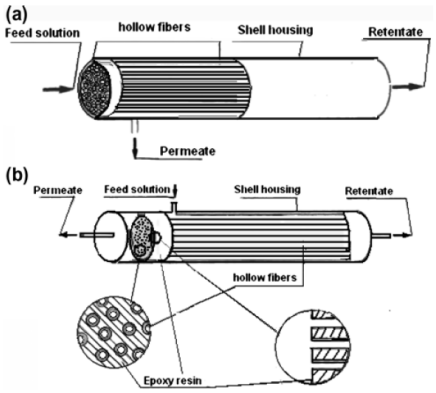

Figure 7: Hollow-fiber membrane module illustration: (a) tube-feed type (b) shell-feed type[20].

Figure 8 shows tubular membrane modules, which are similar to hollow-fiber modules, except with bigger fibers. In a tubular membrane module, generally, fibers are coated on the inside or outside of their porous surface. The fibers are then inserted and sealed in a tubular housing. Controlling concentration polarization effect and fouling is straightforward with this setup owing to superior fluid hydrodynamics [8, 26].

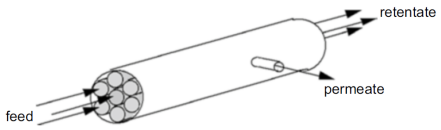

Figure 8: Tubular membrane module illustration[26]

2.5 Membrane contactor

As illustrated in Figure 9, a membrane contactor is a hybrid membrane that acts as a barrier between the gas and liquid phase. However, it does not have control over the rate of the permeates passing through the membrane[8, 27, 28]. Membrane contactors benefit from integrating membrane technology and conventional absorption processes, while selectivity is provided by the solvent[28, 29, 27]. The membrane offers an extensive contact area between phases and non-dispersive contact, which result in improving mass transfer performance and reducing equipment size. High modularity, low operating and capital cost, and controlling liquid and gas flow rates without flooding or foaming are additional advantages of membrane contactors [5, 29, 27, 30]. However, liquid may penetrate pores and cause wetting phenomena, which induce additional mass transfer resistance.

An essential characteristic of the membrane is hydrophobicity, which plays a crucial role in preventing pore wetting phenomena and increasing mass transfer resistance in the membrane. Hydrophobic microporous membranes such as polypropylene (PP), polytetrafluoroethylene (PTFE), or polyvinylidene fluoride (PVDF) are the most frequently used polymers. Moreover, chemical durability is an essential factor in membranes for long-term operations [28]. According to Khaisri et al.[31] PTFE exhibited excellent stability with time, but it is costly. PVDF had almost the same performance as PTFE, despite being

less expensive. However, PP is less hydrophobic and cheaper than the other two polymers.

Dindore et al.[32] investigated the compatibility of different membrane materials with various solvents for CO_2 absorption. It was reported that PP and PTFE are more compatible with organic solvents. The primary benefits of polypropylene are its excellent thermal and chemical resistance, void volume, high porosity, and low cost [27, 29]. However, a membrane with high porosity has large pores and may face wetting phenomena and a decrease in absorption flux[33].

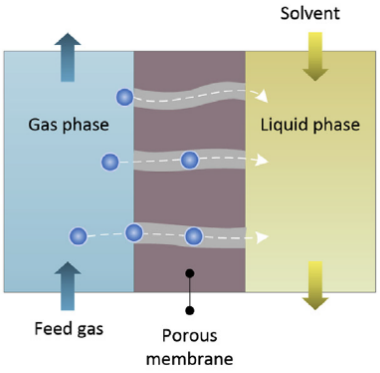

Figure 9: Illustration of a membrane contactor [27]

Apart from all benefits mentioned above, the performance of the membrane contactor is affected by some challenges. The main challenge is the wetting phenomena. Wetting of pores occurs when the membrane's pores become partially or fully wetted by the absorbent. The significant consequence of this phenomenon is that gas molecules can no longer diffuse into the pores. Hence, mass transfer resistance increases dramatically and separation performance reduces. Besides, this problem would have a negative effect on the system performance in long-term operations at high pressures. In large-scale membrane application, failure of pressure drop control through the membrane may result in wetting issue[30]. Membrane characteristics, absorption liquid properties, and membrane compatibility with solvent are essential factors in determining membrane wettability[30, 34, 29].

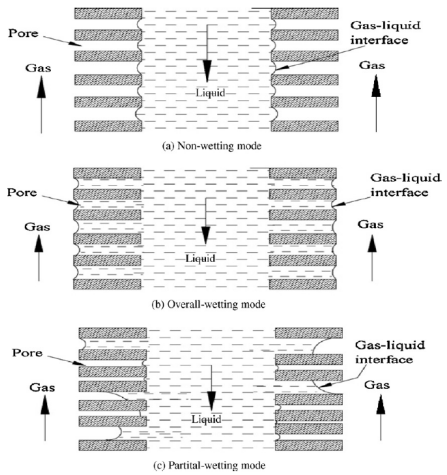

Figure 10: Pore wetting phenomenon in membrane contactor: (a) non-wetted, (b) full-wetted, (c) partially wetted [35]

Critical entry pressure, is defined as the pressure at which liquid enter into the pores of the membrane. The minimum pressure difference that can cause penetration of liquid phase into pores is given by Laplace-Young equation 8:

$$\Delta p = \frac{2\gamma cos\theta}{r_{p,max}} \tag{8}$$

Where θ is the contact angle between liquid and membrane, γ is the surface tension of the liquid phase, and $r_{p,max}$ is the maximum radius of the pores. This equation implies that small pores in a membrane or higher contact angle increase the breakthrough pressure.

Wang et al.[36] explored the effect of the pore wetting phenomenon on CO_2 absorption rate and it has shown that even 5% wettability of pores results in a 20% drop in the overall mass transfer coefficient. In a similar study, Lv et al.[29] reported that wetting phenomena impact the characteristics of PP membrane, as it causes a reduction in hydrophobicity and membrane surface morphology transformation. Qazi et al.[37] also studied the effect of wettability on CO_2 removal process using a hollow fiber membrane contactor and concluded that even 5% wetting results in a 40% reduction in the process efficiency. Rajabzadeh et al.[33], investigated the effect of the ratio of the wetted pore in a membrane on the gas absorption flux. As displayed in Figure 11 when the pores are wetted by 2%, absorption flux is reduced by half. Dalane et al.[38] analyzed wetting phenomena' effect

on the natural gas dehydration process and reported that pore wetting of 50% causes a significant decrease in the water vapor flux to less than 1%. Hence, avoiding penetration of liquid solvents into pores is of great importance. Utilizing composite membranes or asymmetric membranes, surface modifications, optimization of operating conditions, and efficient choice of membrane material and liquid are different strategies to prevent this phenomenon [34].

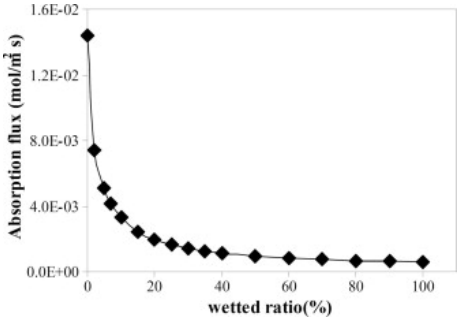

Figure 11: Wettability ratio impact on gas absorption flux [33]

One promising approach for wettability prevention at high pressures in long-term operation is the application of a composite membrane with a dense selective layer. Composite membranes consist of a porous support and a dense layer on top of it. Using a dense layer on a porous membrane hinders liquid penetration and provides stable performance [34, 27, 39]. Although the dense layer adds mass transfer resistance to the system, it offers long-term operations and fewer maintenance [5]. In order to compensate for the effect of the dense layer on the mass transfer resistance, a highly permeable polymer with low thickness can be employed on the porous membrane to minimize the additional resistance.

Zak et al.[40] studied the usage of asymmetric hollow fiber membrane with a polyester carbonate dense layer on it for $CO_2\backslash CH_4$ separation and reported 96% CH_4 purity. Chabanon et al.[41] used poly(1-trimethylsilyl-1-propyne) (PTMS) as the dense layer on PP membrane and reported the effect of dense layer resistance on CO_2 separation performance. The results indicated 90% efficiency in CO_2 removal after ten hours of operation without a wetting problem. Scholes et al.[25] compared three different composite membrane contactors (PTMSP on PP, PIM-1 on PP, and Teflon AF1600 on PP) with a porous polypropylene (PP) membrane to study the overall mass transfer coefficients in each case for CO_2 absorption into MEA. The porous PP membrane was involved in the pore wetting phenomenon.

PTMSP and PIM-1 presented good overall mass transfer coefficients. However, the absorption of water into pores reduced the mass transfer coefficients. In addition, no pore penetration was observed in Teflon AF1600 due to its hydrophobic nature; hence the mass transfer coefficient remained constant. Dalane et al. [38] performed a sensitivity study on the effect of the dense layer thickness on natural gas dehydration. It was reported that when the thickness of the dense layer is 1 μm and its permeability is 100 Barrer, the dense layer is dominant in mass transfer resistance. However, by increasing the permeability, the dense layer thickness does not control the mass transfer resistance. In addition, it is stated that the performance of a dense layer in separation is the same for permeability of larger than 3000 Barrer. Figure 12 shows the results reported for wetting phenomena.

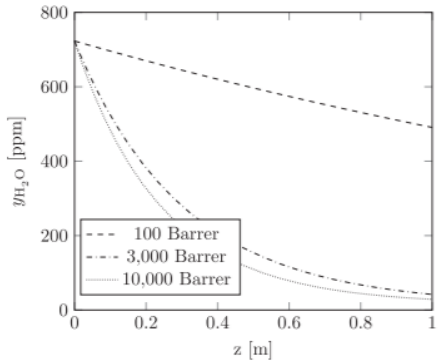

Figure 12: dense layer effect with different permeabilities on natural gas dehydration process [38]

2.5.1 Mass transfer in membrane contactors

There are four different strategies for simulating mass transfer in membrane contactors. Constant overall mass transfer coefficient, resistance in series (1D) model, Convection-diffusion (1D-2D) model and convection-diffusion (2D) model are various approaches for this purpose. Resistance in series is the most widely used model to study the overall mass transfer coefficient. This approach shows three mass transfer resistances in the gas, membrane, and liquid phases. Figure 13 shows an illustration of this model.

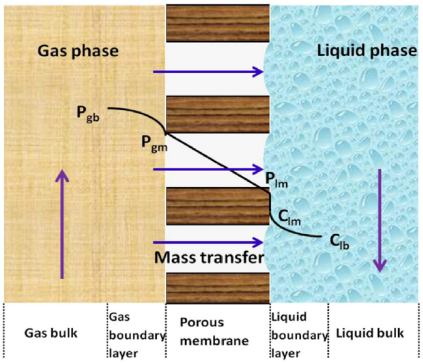

Figure 13: concentration profile in membrane contactor [30]

The mass transfer fluxes at steady state are as given in quation 9:

$$J = k_{g,i}(C_{g,i} - C_{gm,i}) = k_{m,i}(C_{gm,i} - C_{lm,i}) = k_{l,i}(C_{lm,i} - C_{l,i}) \tag{9}$$

Where $k_{g,i}$, $k_{m,i}$ and $k_{l,i}$ are local mass transfer coefficients in the gas phase, membrane and liquid phase. $C_{g,i}$, $C_{gm,i}$, $C_{lm,i}$ and $C_{l,i}$ are concentrations in gas phase, gas-membrane interface, liquid-membrane interface and liquid phase respectively. Hence the overall mass transfer resistance according to resistance in series approach is as follows:

$$\frac{1}{K_{ov}} = \frac{1}{K_g} + \frac{m}{K_l} + \frac{1}{K_m} \tag{10}$$

Where K_{ov} is the overall mass transfer coefficient [m/s], K_g is the local mass transfer coefficient of the gas phase [m/s], K_l is the local mass transfer coefficient of the liquid phase, and m is calculated from equation 11:

$$m = \frac{\gamma_{\mathrm{H_2O}} p^{sat}_{\mathrm{H_2O}}}{\varphi_{\mathrm{H_2O}} p} \tag{11}$$

Where$\gamma_{\mathrm{H_2O}}$ and $\varphi_{\mathrm{H_2O}}$ are the activity coefficient and fugacity coefficient of water, respectively. $\mathrm{p^{sat}_{H_2O}}$ is the saturated water vapor pressure [kPa] and p is the total pressure [kPa].

Chapter 3

3 Experiments

3.1 Chemicals and materials

Teflon AF2400 was purchased from Chemours, and Perfluorrohexane (FC-72) was supplied from Kemi-Intressen AB (Sweden). Triethylene Glycol 99% was purchased from Sigma-Aldrich. Tubular polypropylene (PP) membrane support with inner diameter of 1.67 [mm] and outer diameter of 2.5 [mm] was purchased from Membrana 3M.As shown in Figure 15, the fiber has an asymmetric structure. The size of the pores on the inside of the fiber is smaller than those on the outside. Instant epoxy glue LOCTITE 3090 and epoxy adhesive LOCTITE EA 9483 were purchased from Henkel. All chemicals were used the way they were received without any purification. The methane bottle with a purity of 99.999% was purchased from AGA, Norway.

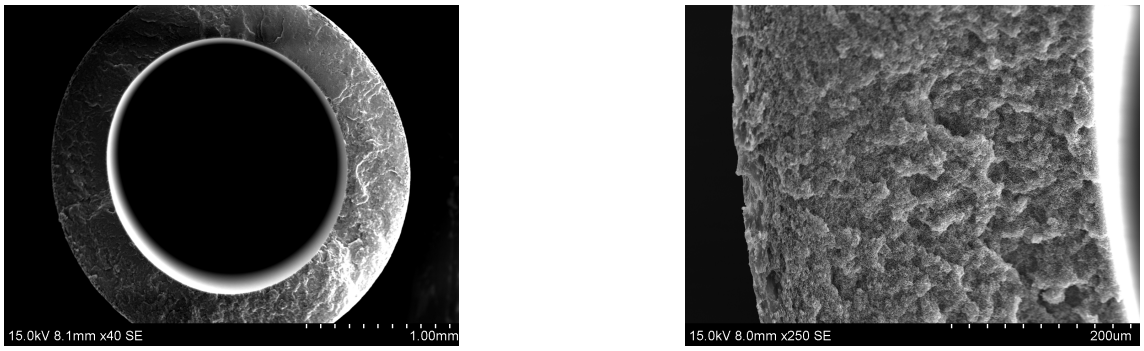

Figure 14: Polypropylene fiber stucture

3.2 Membrane module

The tubular membrane module (Figure 15) was fabricated by inserting five PP fibers in a stainless steel tube with an inside diameter of 6.6 [cm]. The effective length of the membrane module was 26 [cm], and epoxy resin was used for sealing both sides of the membrane module. Five fibers in each module with an inner diameter of 1.67 [mm],

provided an effective area of 68.2 [cm^2]. Table 4 displays a summary of the module specifications.

Module Specifications	
Fiber outer diameter (mm)	2.50
Fiber inner diameter (mm)	1.67
Number of fibers	5.00
Fiber inner area (cm^2)	13.64
Fiber outer area (m^2)	20.41
Module length (cm)	26.00
Module packing density	617.28
Module inner diameter (cm)	6.60

Table 4: The prepared tubular module specifications

Figure 15: The in-house membrane module

3.3 Synthesis and membrane preparation

An adequate amount of Teflon AF2400 was added to solvent FC-72 to make a 1 wt% solution of AF2400 at room temperature. The solution was stirred overnight to dissolve in FC-72 until a homogeneous solution was obtained. The fibers were coated from the inside. Prior to being coated, fibers were installed within the module and both sides were blocked by instant epoxy glue to prevent the subsequent adhesive from penetrating the fibers. When the instant glue dried, the module was sealed on both sides using epoxy glue (Figure 16). At least 8 hours was required for the epoxy to dry thoroughly. The excess dried glue outside the module was removed, and inner of the fibers were inspected for glue penetration and blockage.

Figure 16: The procedure of sealing the module from both ends using epoxy glue

Afterward, as shown in figure 17, the module was fixed vertically and connected to the peristaltic pump from the downside, and the pump's motor speed was set at 30 rpm. The pressure of the shell side remained at atmospheric pressure. Initially, FC-72 solvent was poured into the module as a pore-filling agent. Subsequently, the solution was poured from the topside and drained by the pump from the downside. Then the module was left in the same position for two hours while connected to a compressed air stream to accelerate the drying period and remove excess solution from the fibers. Furthermore, the module was turned upside down and coated again, following the same procedure as in the case of the previous step. Then for heat treatment, the module was placed in a ventilation oven for two hours at 45°C.

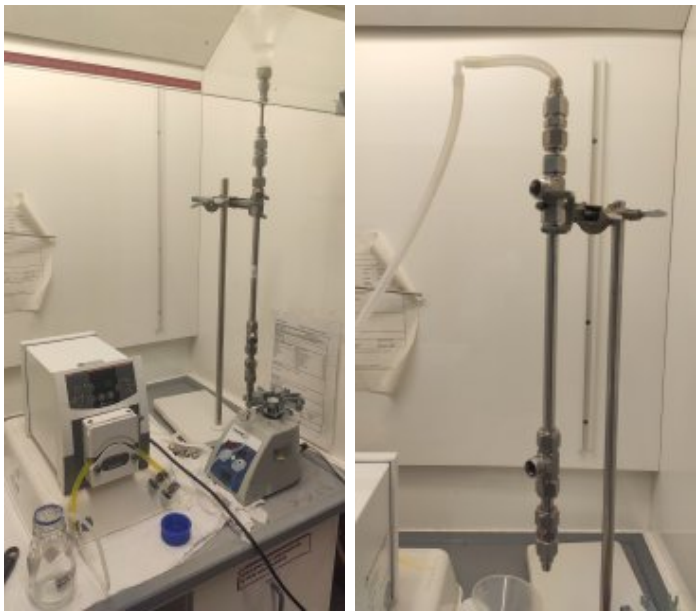

Figure 17: Coating 1 wt% Teflon AF2400 solution in FC-72 solvent on PP fibers

3.4 Morphological characterization

SEM was employed to measure the thickness of the dense layer coated on the PP porous fibers and check the defects that may appear in the selective layer. Hitachi TM3030 and Hitachi SU-6600 SEM instruments were used to explore the morphology characteristics of the membrane by capturing a cross-sectional SEM image. For preparing SEM samples, three pieces from different parts of the fibers were cut to ensure that the thickness of the dense layer was uniform. Then the samples were immersed in nitrogen liquid for a few seconds and fractured. Adhesive carbon foil was used to stick the samples to the sample holder. Before taking the SEM image, the samples were placed in The Quorum Q150 ES sputter coater instrument and were coated with gold at a pressure of 1.3 atm for 40 seconds.

3.5 Single gas permeation setup

Figure 18 shows the flow diagram of the single gas permeation setup. This experiment aimed to ensure whether the dense layer is completely coated inside the fibers. For this purpose, the permeability and selectivity of different gases through the membrane were

examined. In dense membranes, solution-diffusion is the predominant transport mechanism; hence, the permeability of the gases could well be calculated using the following equation:

$$P_i = \frac{V_d l}{\Delta p A R T}[\frac{dp}{dt} - (\frac{dp}{dt})_{leak}] \tag{12}$$

Where P_i is the gas permeability [Barrers] (1 [Barrers] = 10^{-10} [cm^3(STP)cm/$cm^2s^1cmHg^1$]), l is the membrane thickness [cm], p is the pressure difference through the membrane [cmHg], dp/dt is the steady-state increase in pressure [cmHg/s], $(dp/dt)_{leak}$ is the possible leakage [cmHg/s], V_d is the downstream volume [cm^3], A is membrane area [cm^2], T is the operating temperature [K], and R is the gas constant (0.2784 [cm^3cmHg/cm^3(STP)K]). As indicated in the preceding chapter, membrane selectivity is determined using equation13:

$$\alpha_{i/j} = \frac{P_i}{P_j} \tag{13}$$

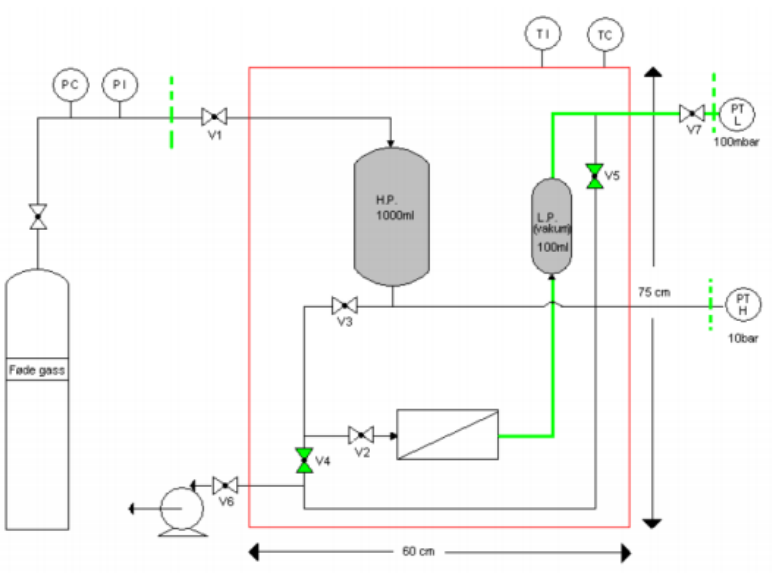

Figure 18: Single gas permeation setup flow diagram

The membrane's selectivity and permeability were evaluated in a single gas permeation setup. The permeate flux was calculated by measuring the pressure difference across the membrane. When the module was mounted in the setup, it was exposed to a vacuum

overnight to remove any penetrates. Furthermore, a leak test was conducted to determine the leakage rate by closing the valve on the permeate side while keeping vacuum conditions on the other side. The valve on the shell side was closed and the high-pressure tank was filled with the feed gas. Then the valve between the tank and membrane was opened, while the gas feed was introduced into the system at a specific pressure. Hence, the pressure in the permeate side started to increase drastically, which was recorded using LabVIEW software. The data were analyzed to determine the steady-state condition, where (dp/dt) was constant. The experiment was carried out for CO_2 and N_2 gases at the pressure of 1 and 2 [bar]. The permeability and selectivity of carbon dioxide and nitrogen were measured to ensure that the dense layer thoroughly covered the fibers' inner surface.

Test	Gas	Pressure (bar)	Temperature (°C)
1	N_2	1	25
2	N_2	2	25
3	CO_2	1	25
4	CO_2	2	25

Table 5: Data experiments for measuring permeability and selectivity of CO_2 and N_2 in Teflon AF2400

3.6 Membrane contactor testing setup

Figure 19 shows the flow diagram of the membrane contactor setup by Ahmadi et al.[5]. The prepared module with an effective area of 68.2 [cm^2] was mounted in an isothermal oven. Dried gas flowed into a humidifier to mix with water vapor on the gas side of the setup. A dew point sensor was employed after the humidifier to measure the wet gas dew point in the outlet of the humidifier. JULABO water bath was used to control the water temperature inside the humidifier. Pre-heating bath was used to prevent water condensation while reaching the module due to temperature difference with ambient temperature. Another dew point sensor was installed after the module to measure the outlet gas dew point. On the liquid side, a piston pump was employed to pump TEG to the system. A manual back pressure controller was employed for tuning the liquid side pressure. The

gas pressure was assigned to 0.5 bar less than the liquid side average pressure from downstream and upstream of the module. LabVIEW Software was used for data collection and controlling the operating conditions. Three sets of experiments were arranged: First, the effect of liquid flow rate on the water flux was explored. Besides, the effect of pressure and gas flow rate on the water vapor flux was examined. The temperature was kept at 35 °C in all experiments.

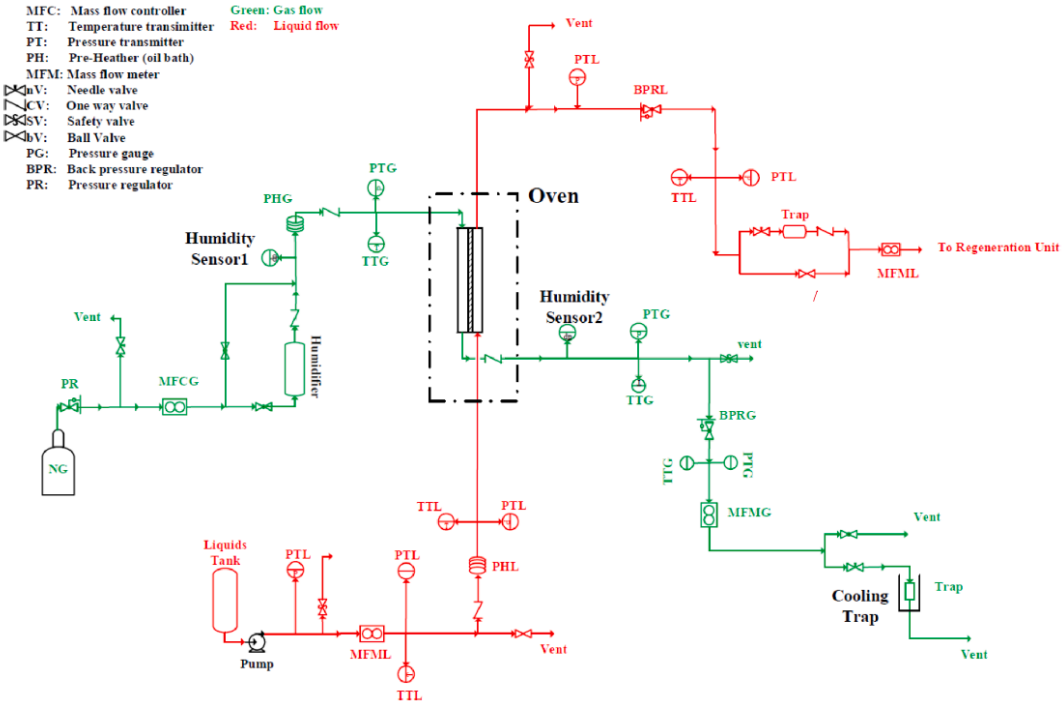

Figure 19: The flow diagram of membrane contactor setup [5]

3.7 Operating parameters

3.7.1 Liquid flow rate effect

The effect of liquid flow rate on water vapor flux was investigated. The goal of this experiment was to explore whether a high liquid flow rate increases water vapor flux across the membrane. Moreover, it was aimed to investigate the impact of very low liquid flow rates on water vapor flux. The controller, which was used for the pump on the liquid side, did not work appropriately. Due to the fluctuation in liquid flow rate imposed by the pump, liquid flow rate of lower than 800 [gr/h] was impossible to achieve. To solve this issue,

the bypass line from the pump to the tank was partially opened to decrease the liquid flow entering the membrane. However, it made pressure control arduous. As shown in table 8, at the pressure of 7 [bar] and gas flow rate of 300 [ml/min] and temperature of 35 [°C], three points were chosen to examine the water vapor flux at different liquid flow rates.

Test	F_L(g/h)	F_G(ml/min)	Pressure (bar)	Temperature (°C)
1	1500	300	7.0	35
2	200	300	7.0	35
3	50	300	7.0	35

Table 6: Effect of liquid flow rate on water flux tests

3.7.2 Gas flow rate and pressure effect

In order to investigate operating parameters' effects on water flux, the design of experiments (DOE) was employed. The effects of gas flow rate and pressure were evaluated, while the temperature was kept at 35 [°C] and the liquid flow rate was set to the lowest possible amount without fluctuations, at 1500 [g/h]. Considering limitations on flow meter readings and safety aspects of operating at high pressures, three points were chosen to investigate the impact of each parameter. Gas flow rate was chosen to change from 50 to 2000 [ml/min] and pressure from 2 to 7 [bar], while the gas flow rate and pressure of center point were selected to 300 [ml/min] and 3.5 [bar], respectively. Table 7 shows the values of gas flow rates and pressures chosen for the experiments.

operating parameters	lower bound	center	upper bound
Pressure (P) (bar)	2	3.5	7.0
Gas Flow rate (F_G)(ml/min)	50	300	2000

Table 7: Pressure and gas flow rate effect

The average flux of water vapor was calculated by following equation 14:

$$j = \frac{({y_A}^{in} - {y_A}^{out})F_G}{A_m}(\frac{pM_w}{R_{const}T})(\frac{60(\text{min/h})1.013(\text{atm/bar})}{1000(\text{ml/L})}) \tag{14}$$

where j is water flux [g/m^{2}h], ${y_A}^{in}$ and ${y_A}^{out}$ are water vapor mole fraction on the inlet and outlet of the membrane, F_G is the gas flow rate [ml/min], A_m is the membrane area [m^2], p is the total pressure [bar], M_w is the water molecular weight [g/mol] and R_{const} is the gas constant [atm L/mol K].The dew point of the gas flow in the outlet under steady state condition was recorded. Aspen HYSYS software was used to convert dew points to water mole fraction using sour PR equation of state.

3.8 Durability validation test

Long-term performance of membrane contactors may result in changes in morphological characterization and wetting phenomena and hence decrease water vapor flux. Therefore, the membrane was tested continuously in a long-term operation for 30 days. Temperature, pressure, liquid flow rate and gas flow rate were kept at 35 [°C], 5 [bar], 1500 [g/h] and 300 [ml/min], respectively during this period. For validation, 3 random points with different pressure and gas flow rate were chosen. The membrane was tested under these 3 conditions with different gas flow rates and pressure; before and after long-term operation. The temperature and liquid flow rate in validation tests were set to 35 [°C] and 1500 [g/h], respectively. In table 8 the random values of pressure and gas flow rate for each point are displayed.

Test	Gas flow rate (ml/min)	Pressure (bar)
1	800	3
2	1600	5
3	400	5

Table 8: Randomly selected values for validation tests

Chapter 4

4 Results and Discussion

4.1 Morphological characterization result

The thickness of the dense layer and the membrane morphology was further analyzed with SEM images. Figure 20 shows the SEM image of cross-section Teflon AF2400 on PP support fiber. Two layers are visible in this image, the spongy part of the PP membrane and the dense layer of Teflon AF2400 on its inner surface. No defect was apparent on the surface of the support and the PP support was not damaged. The dense layer seemed uniform over the whole area and an average Thickness of 2.77 ± 0.05 [μm] was obtained.

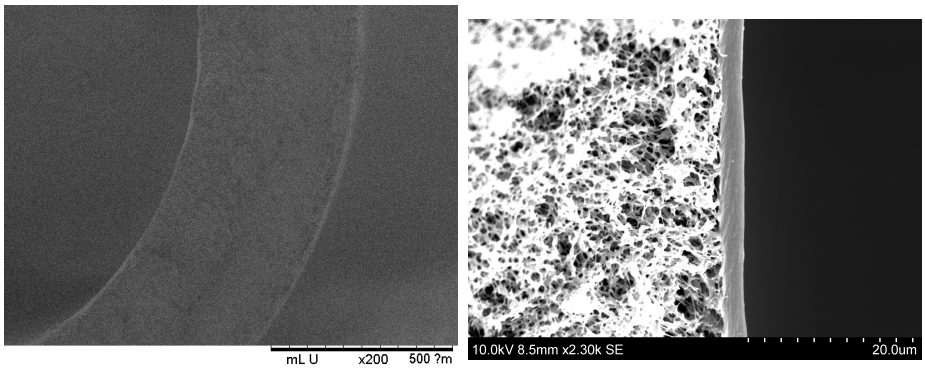

(a) the coated inner surface of the fiber **(b)** coated layer thickness

Figure 20: SEM image of Teflon AF2400/PP composite membrane

4.2 Gas permeation and selectivity

Since diffusivity is dominant in the gas transport mechanism in glassy polymers and is reliant on molecular gas size, gas molecules with smaller molecular sizes have lower permeability. According to the reported data provided by Jansen et al.[14], Teflon AF2400 membrane exhibited CO_2 and N_2 permeabilities of 2980 and 580 [Barrer] at 1 [bar] and 25 [°C], respectively. Hence the selectivity of Teflon AF2400 for CO_2 over N_2 is 5.1. The

producer, Dupont Co., reported almost similar permeability values as well. Moreover, it is reported that pressure variation does not have an influence on the permeability of these two gases[42]. The results of permeability and selectivity of AF2400 membrane for carbon dioxide and nitrogen at a pressure of 1 and 2 [bar] are presented in table 9. The predicted permeabilities and selectivities are in good agreement with the reported data[14], ensuring that the inner surface of the fibers was completely and appropriately coated.

Pressure (bar)	Temperature (°C)	$P_{N_2}(Barrer)$	$P_{CO_2}(Barrer)$	α_{CO_2/N_2}
1	25	550	2940	5.3
2	25	580	3030	5.2

Table 9: Permeability and selectivity of Teflon AF2400 at 25 °C and 1 and 2 bar of feed pressure for CO_2 and N_2

4.3 Liquid flow rate effect

The effect of liquid flow rate was examined while the gas flow rate, pressure and temperature were kept at 300 [ml/min], 7 [bar], and 35 [°C], respectively and three different liquid flow rates of 50 [g/h], 200 [g/h] and 1600 [g/h] were employed. This experiment aimed to study the liquid flow rate effect on water flux in the membrane. In table 10, the operating conditions, liquid velocity, the inlet and outlet dew points, and the water vapor mole fraction in the gas phase are presented.

F_L(g/h)	u_L(cm/s)	P (ml/min)	$DP_{inlet}(°C)$	$y_{inlet}(ppmv)$	$DP_{outlet}(°C)$	$y_{outlet}(ppmv)$
54.56	0.12	7.04	19.53	3300	−6.96	500
260.65	0.57	7.04	19.41	3300	−6.93	400
1581.41	3.44	7.05	19.93	3700	−7.01	500

Table 10: Liquid flow rate effect on water vapor flux

Plot 21 displays water vapor flux for different liquid flow rates. As shown in the plot, water flux changes through the membrane did not significantly affect the outlet water dew

point. Hence, it can be concluded that mass transfer resistance is negligible in the liquid phase. The slight change in the rate of liquid flow could be attributable to fluctuations in liquid flow rate as well as enhanced pressure drop across the membrane as the liquid flow rate rises. In addition, the transfer rate from the boundary layer to the bulk phase is mainly controlled by diffusion. High TEG viscosity ($\approx$ 26 cp at 35 °C) and low diffusion of water into TEG in the liquid boundary layer reduce water transport from the boundary layer to the bulk phase. In addition, the equilibrium obtained between the output gas stream and the intake liquid contributes to the modest dependence of the performance of the membrane on the liquid flow rate. As a result, the liquid flow rate became less effective on water flux through the membrane. Similar results were also reported regarding the influence of liquid flow rate on the performance of Teflon AF2400 hollow fiber and flat-sheet membrane contactors [38, 5]. Moreover, As seen in the table, even though the liquid velocity reduced to 0.12 [cm/s], the changes in the outlet water vapor fraction are insignificant. Therefore, it can be concluded that decreasing the liquid flow rate to its minimum value is beneficial and results in reduction in solvent consumption and operational costs.

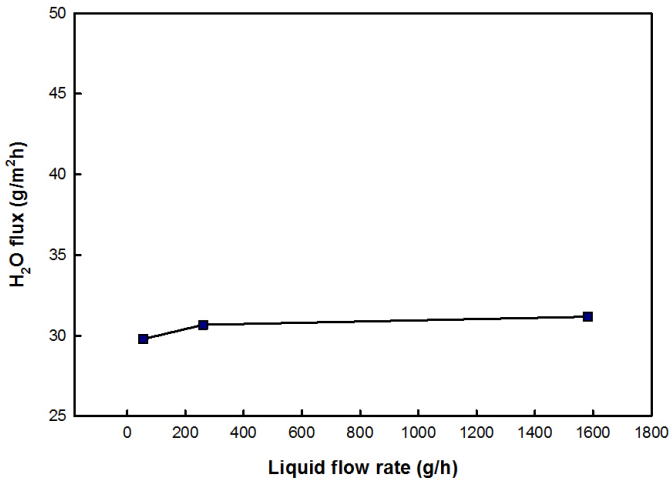

Figure 21: Water flux as a function of liquid flow rate

4.4 Gas flow rate effect

The effect of gas flow rate was investigated when the pressure, liquid flow rate and temperature set to 3.5 [bar], 1500 [gr/h], and 35 [°C], respectively. Table 11 displays the obtained experimental results. As presented in the table, by increasing gas flow rate from 50 [ml/min] to 2000 [ml/min], the outlet dew point raised from −17.29 [°C] to 15.00 [°C]. Increasing the outlet dew point is due to the fact that increasing the gas flow rate reduces the gas phase residence time in the membrane contactor. It can be seen that the effect of pressure on the inlet water content in the gas phase is more pronounced than the gas flow rate. Since the pressure is almost identical for all cases while the gas flow rate changes, the inlet dew point is the same. However, the pressure difference in each experiment has an influence on the inlet water flux.

F_G(ml/min)	P (bar)	$DP_{inlet}(^{\circ}C)$	$y_{inlet}(ppmv)$	$DP_{outlet}(^{\circ}C)$	$y_{outlet}(ppmv)$
30.61	3.57	19.51	7100	−17.29	100
278.04	3.58	19.53	7200	1.90	2300
2032.50	3.59	19.30	7000	15.00	5600

Table 11: The effect of gas flow rate on water vapor flux

Plot 22 displays water vapor flux as a function of gas flow rate. As seen from the plot, the water flux through the membrane increased by increasing the gas flow rate. Lowering flow rate reduces the driving force along the membrane; however, raising the gas flow rate flattens the water concentration profile along the membrane in the gas phase, providing a higher driving force.

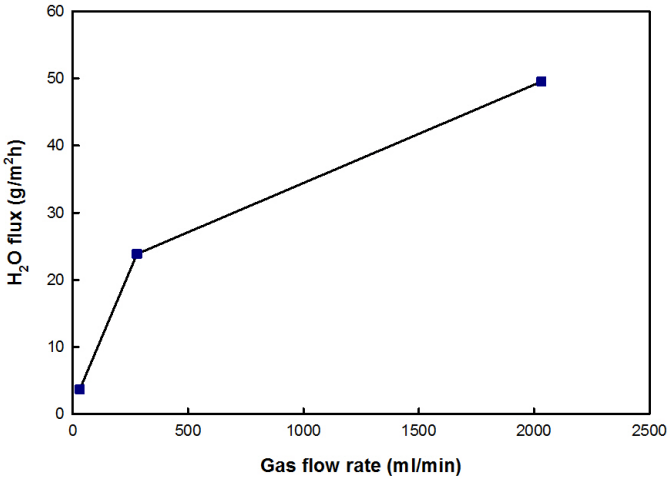

Figure 22: Water flux as a function of gas flow rate

4.5 Pressure effect

The effect of pressure was investigated at constant temperature of 35 °c, gas flow rate of 300 [ml/min] and liquid flow rate of 1500 [g/h] (Table 12). As shown in plot 21, water flux increased with an increase in pressure. Water mole fraction was reduced by increasing total pressure. However, partial inlet pressure remained almost the same for all experiments. Hence, an increase in pressure has a negligible effect on the partial pressure of water in the inlet gas. It is well-known that increasing pressure gives rise to a higher absorption rate. Therefore, the effect of pressure on absorption rate should be taken into account. An increase in pressure causes higher absorption in the liquid phase and reduced outlet dew point.

F_G(ml/min)	P (bar)	$DP_{inlet}(°C)$	$y_{inlet}(ppmv)$	$DP_{outlet}(°C)$	$y_{outlet}(ppmv)$
292.32	2.22	19.93	12700	6.73	6000
278.04	3.58	19.86	7200	1.90	2300
276.09	7.05	19.93	3700	−7.01	500

Table 12: Experimental results of the effect of pressure on water vapor flux

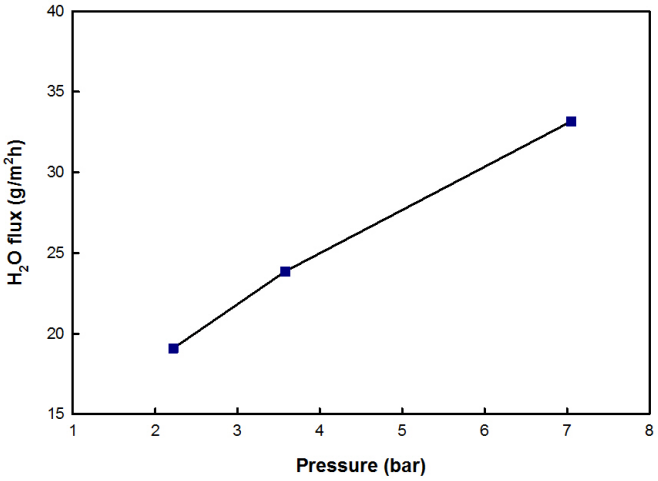

Figure 23: Water flux as a function of pressure

4.6 Validation tests results

The durability test of the membrane for the long-term operation was performed continuously under a specific operating condition for 30 days. Before the long-term durability test, three operating conditions were randomly selected to be tested. The experiments were repeated after long-term operation to ensure the constituency of the results. Temperature and liquid flow rate were set to 35 [°C] and 1500 [g/h]. The results are displayed in table 13.

Test	F_G(ml/min)	P (bar)	$DP_{outlet}(^{\circ}C)$	$y_{outlet}(ppmv)$	J(g/m^{2}h)	Deviation(%)
1^a	384.04	5.11	0.61	1400	36.54	
1^b	385.43	5.18	0.62	1400	35.96	1.6
2^a	773.64	3.19	11.88	5400	40.87	
2^b	789.27	3.21	12.23	5600	36.64	10.3
3^a	1596.87	5.16	13.26	3300	74.17	
3^b	1607.94	5.18	13.48	3400	66.90	9.8

Table 13: Validation tests results: (a) denotes to tests before long-term operation, (b) denotes to tests repeated after long-term operation.

The results show that after 30 days of operation, there was a maximum of 10.3% reduc-

tion in the water flux through the membrane. By examining the membrane morphology after the durability test and the primitive membrane, as shown in Figure 24, the pores were kept intact and no deformation was observed in the structure of the porous support and selective layer. However, the results from the random tests show a drop in the flux, indicating that during the durability test, TEG penetration through the pores was the main reason for this deviation. Concerning the data points, the deviation decreased for the tests performed at higher pressure and low gas flow rate. This reduction could be due to an increased absorption rate in the liquid phase at higher pressures.

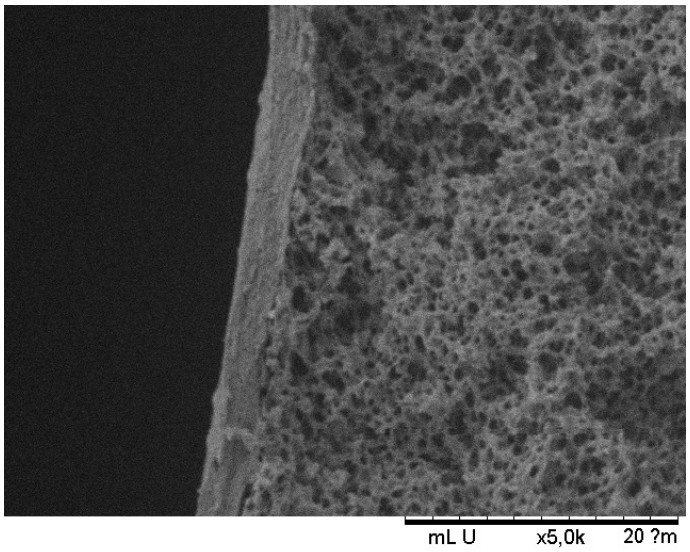

(a) membrane after durability test

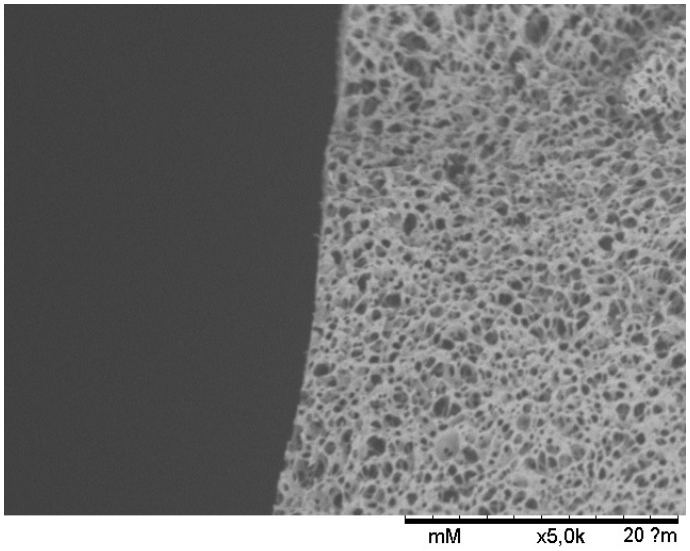

(b) membrane before durability test

Figure 24: The SEM images of membrane before and after durability test

Chapter 5

5 Conclusion

This project aimed to fabricate and improve the performance of a tubular membrane module for natural gas dehydration. The fibers were coated with a solution of 1 wt% Teflon AF2400 in solvent FC-72 while inserted in a tubular module that was sealed at both ends. The thickness and the morphological characteristics of this membrane were examined by SEM. The selectivity of the dense layer of carbon dioxide over nitrogen was obtained using a single gas permeation test. The module was mounted in the gas dehydration setup where TEG was used as the absorbent. The effects of liquid flow rate, gas flow rate and pressure on water vapor removal from the gas phase were evaluated and analyzed. Besides, validation tests performed before and after long-term operation in order to determine the effect of membrane durability on water flux.

The composite membrane was made from a PP support and 1 wt% Teflon AF2400 dense layer on the inside surface of the fibers. FC-72 was used as a pore-filling agent. The study of morphological characteristics of the fibers showed a thickness of 2.77 ± 0.05 $[\mu m]$ of Teflon AF2400 without penetration of the solution into the pores. Besides, the module was installed in a single gas permeation setup to investigate the selectivity of the fabricated module of CO_2 / N_2. The results showed a selectivity of 5.3 and 5.2 at a pressure of 1 and 2 bar, respectively, which is in good agreement with experimentally reported data in the literature.

The effects of operating conditions were performed in the gas dehydration setup. The liquid flow rate variation did not remarkably affect water flux through the membrane. When the influence of gas flow rate is considered, a higher gas flow rate is desired since it increases water vapor flux through the membrane. In addition, an increase in pressure has a significant effect on the performance of the separation.

The results of membrane performance presented a maximum of 10.3% reduction in gas flow rate after operating for 30 days continuously. The SEM images of the fabricated fibers

did not display deformation or defects in the membrane. However, reduction in gas flow rate exhibited absorbent penetration into the pores. To conclude, membrane contactor technology ensures promising results in removing water vapor from Natural gas. A dense layer of Teflon AF2400 exhibited outstanding performance for gas separation processes. In further work, however, consideration should be given to improving the characteristics of the membrane in order to withstand operating conditions over an extended period of time.

Bibliography

[1] Marco Tagliabue et al. 'Natural gas treating by selective adsorption: Material science and chemical engineering interplay'. In: *Chemical Engineering Journal* 155.3 (2009), pp. 553–566. DOI: https://doi.org/10.1016/j.cej.2009.09.010.

[2] Kátilla M.C. Santos et al. 'Natural gas dehydration by adsorption using MOFs and silicas: A review'. In: *Separation and Purification Technology* 276 (2021), p. 119409. DOI: https://doi.org/10.1016/j.seppur.2021.119409.

[3] Zong Yang Kong et al. 'Revamping existing glycol technologies in natural gas dehydration to improve the purity and absorption efficiency: Available methods and recent developments'. In: *Journal of Natural Gas Science and Engineering* 56 (2018), pp. 486–503. DOI: https://doi.org/10.1016/j.jngse.2018.06.008.

[4] Kristin Dalane et al. 'Potential applications of membrane separation for subsea natural gas processing: A review'. In: *Journal of Natural Gas Science and Engineering* 39 (2017), pp. 101–117. DOI: https://doi.org/10.1016/j.jngse.2017.01.023. URL: https://www.sciencedirect.com/science/article/pii/S187551001730032X.

[5] Mahdi Ahmadi et al. 'Subsea natural gas dehydration in a membrane contactor with turbulence promoter: An experimental and modeling study'. In: *Chemical Engineering Journal* 404 (2021), p. 126535. DOI: https://doi.org/10.1016/j.cej.2020.126535.

[6] Richard W. Baker and Kaaeid Lokhandwala. 'Natural Gas Processing with Membranes: An Overview'. In: *Industrial & Engineering Chemistry Research* 47.7 (2008), pp. 2109–2121. DOI: 10.1021/ie071083w.

[7] Lloyd M. Robeson. 'The upper bound revisited'. In: *Journal of Membrane Science* 320.1 (2008), pp. 390–400. DOI: https://doi.org/10.1016/j.memsci.2008.04.030.

[8] R. W. Baker. *Membrane Technology and Applications*. John Wiley Sons, Ltd, 2012. DOI: https://doi.org/10.1002/0470020393.ch1.

[9] M. Mulder. *Basic Principles of Membrane Technology*. Springer Netherlands, 1996. DOI: https://doi.org/10.1007/978-94-009-1766-8.

[10] R.J.R. Uhlhorn, K. Keizer and A.J. Burggraaf. 'Gas and surface diffusion in modified -alumina systems'. In: *Journal of Membrane Science* 46.2 (1989), pp. 225–241. DOI: https://doi.org/10.1016/S0376-7388(00)80337-3.

[11] Haiqing Lin et al. 'Dehydration of natural gas using membranes. Part I: Composite membranes'. In: *Journal of Membrane Science* 413-414 (2012), pp. 70–81. DOI: https://doi.org/10.1016/j.memsci.2012.04.009.

[12] H. Feng, H. Zhang and L. Xu. 'Polymeric Membranes for Natural Gas Conditioning'. In: *Energy Sources, Part A: Recovery, Utilization, and Environmental Effects* 29.14 (2007), pp. 1269–1278. DOI: 10.1080/00908310600623611.

[13] Lloyd M. Robeson et al. 'Comparison of transport properties of rubbery and glassy polymers and the relevance to the upper bound relationship'. In: *Journal of Membrane Science* 476 (2015), pp. 421–431. DOI: https://doi.org/10.1016/j.memsci.2014.11.058.

[14] Johannes Carolus Jansen, Karel Friess and Enrico Drioli. 'Organic vapour transport in glassy perfluoropolymer membranes: A simple semi-quantitative approach to analyze clustering phenomena by time lag measurements'. In: *Journal of Membrane Science* 367.1 (2011), pp. 141–151. ISSN: 0376-7388. DOI: https://doi.org/10.1016/j.memsci.2010.10.063. URL: https://www.sciencedirect.com/science/article/pii/S037673881000846X.

[15] V. Smuleac et al. 'Novel perfluorinated polymer-based pervaporation membranes for the separation of solvent/water mixtures'. In: *Journal of Membrane Science* 352.1 (2010), pp. 41–49. DOI: https://doi.org/10.1016/j.memsci.2010.01.058.

[16] Hong Zhang and Stephen G. Weber. 'Teflon AF Materials'. In: *Fluorous Chemistry*. Springer Berlin Heidelberg, 2012, pp. 307–337. DOI: 10.1007/128_2011_249.

[17] Hong Zhang, Abul Hussam and Stephen G. Weber. 'Properties and Transport Behavior of Perfluorotripentylamine (FC-70)-Doped Amorphous Teflon AF 2400 Films'. In: *Journal of the American Chemical Society* 132.50 (2010), pp. 17867–17879. DOI: 10.1021/ja1075647.

[18] A.M Polyakov, L.E Starannikova and Yu.P Yampolskii. 'Amorphous Teflons AF as organophilic pervaporation materials: Transport of individual components'. In: *Journal of Membrane Science* 216.1 (2003), pp. 241–256. DOI: https://doi.org/10.1016/S0376-7388(03)00077-2.

[19] https://www.sigmaaldrich.com/NO/en/product/aldrich/469629. Online; accessed 14 December 2021.

[20] Xing Yang et al. 'Membrane module design and dynamic shear-induced techniques to enhance liquid separation by hollow fiber modules: a review'. In: *Desalination and Water Treatment* 51.16-18 (2013), pp. 3604–3627. DOI: 10.1080/19443994.2012.751146.

[21] Chun Feng Wan et al. 'Design and fabrication of hollow fiber membrane modules'. In: *Journal of Membrane Science* 538 (2017), pp. 96–107. DOI: https://doi.org/10.1016/j.memsci.2017.05.047.

[22] Joerg Balster. 'Plate and Frame Membrane Module'. In: *Encyclopedia of Membranes*. Ed. by Enrico Drioli and Lidietta Giorno. Berlin, Heidelberg: Springer Berlin Heidelberg, 2015, pp. 1–3. ISBN: 978-3-642-40872-4. DOI: 10.1007/978-3-642-40872-4_1584-1.

[23] J. Schwinge et al. 'Spiral wound modules and spacers: Review and analysis'. In: *Journal of Membrane Science* 242.1 (2004), pp. 129–153. DOI: https://doi.org/10.1016/j.memsci.2003.09.031.

[24] S. Lee. 'Performance Comparison of Spiral-Wound and Plate-and-Frame Forward Osmosis Membrane Module'. In: *Membranes* 10.11 (2020), p. 318. DOI: https://doi.org/10.3390/membranes10110318.

[25] Colin A. Scholes et al. 'Comparison of thin film composite and microporous membrane contactors for CO2 absorption into monoethanolamine'. In: *International Journal of Greenhouse Gas Control* 42 (2015), pp. 66–74. DOI: https://doi.org/10.1016/j.ijggc.2015.07.032.

[26] Ahmad Fauzi Ismail, Kailash Chandra Khulbe and Takeshi Matsuura. 'Membrane Modules and Process Design'. In: *Gas Separation Membranes: Polymeric and Inorganic*. Cham: Springer International Publishing, 2015, pp. 221–240. DOI: 10.1007/978-3-319-01095-3_5.

[27] Utjok W.R. Siagian et al. 'Membrane-based carbon capture technologies: Membrane gas separation vs. membrane contactor'. In: *Journal of Natural Gas Science and Engineering* 67 (2019), pp. 172–195. DOI: https://doi.org/10.1016/j.jngse.2019.04.008.

[28] Zhang Ze and J Sx. 'Hollow fiber membrane contactor absorption of CO2 from the flue gas: review and perspective'. In: *Glob. Nest J* 16 (2014), pp. 355–374.

[29] 'Wetting of polypropylene hollow fiber membrane contactors'. In: *Journal of Membrane Science* 362.1 (2010), pp. 444–452. DOI: https://doi.org/10.1016/j.memsci.2010.06.067.

[30] Shuaifei Zhao et al. 'Status and progress of membrane contactors in post-combustion carbon capture: A state-of-the-art review of new developments'. In: *Journal of Membrane Science* 511 (2016), pp. 180–206. DOI: https://doi.org/10.1016/j.memsci.2016.03.051.

[31] Sakarin Khaisri et al. 'Comparing membrane resistance and absorption performance of three different membranes in a gas absorption membrane contactor'. In: *Separation and Purification Technology* 65.3 (2009), pp. 290–297. DOI: https://doi.org/10.1016/j.seppur.2008.10.035.

[32] V.Y. Dindore et al. 'Membrane–solvent selection for CO2 removal using membrane gas–liquid contactors'. In: *Separation and Purification Technology* 40.2 (2004), pp. 133–145. DOI: https://doi.org/10.1016/j.seppur.2004.01.014.

[33] Saeid Rajabzadeh et al. 'Effect of membrane structure on gas absorption performance and long-term stability of membrane contactors'. In: *Separation and Purification Technology* 108 (2013), pp. 65–73. DOI: https://doi.org/10.1016/j.seppur.2013.01.049.

[34] Sanaz Mosadegh-Sedghi et al. 'Wetting phenomenon in membrane contactors – Causes and prevention'. In: *Journal of Membrane Science* 452 (2014), pp. 332–353. DOI: https://doi.org/10.1016/j.memsci.2013.09.055.

[35] A. Mansourizadeh and A.F. Ismail. 'Hollow fiber gas–liquid membrane contactors for acid gas capture: A review'. In: *Journal of Hazardous Materials* 171.1 (2009), pp. 38–53. DOI: https://doi.org/10.1016/j.jhazmat.2009.06.026.

[36] R. Wang et al. 'Influence of membrane wetting on CO2 capture in microporous hollow fiber membrane contactors'. In: *Separation and Purification Technology* 46.1 (2005), pp. 33–40. DOI: https://doi.org/10.1016/j.seppur.2005.04.007.

[37] Sohaib Qazi et al. 'CO2 capture in a hollow fiber membrane contactor coupled with ionic liquid: Influence of membrane wetting and process parameters'. In: *Separation and Purification Technology* 233 (2020), p. 115986. DOI: https://doi.org/10.1016/j.seppur.2019.115986.

[38] Kristin Dalane et al. 'Membrane contactor for subsea natural gas dehydration: Model development and sensitivity study'. In: *Journal of Membrane Science* 556 (2018), pp. 263–276. DOI: https://doi.org/10.1016/j.memsci.2018.03.033.

[39] Bouchra Belaissaoui and Eric Favre. 'Novel dense skin hollow fiber membrane contactor based process for CO2 removal from raw biogas using water as absorbent'. In: *Separation and Purification Technology* 193 (2018), pp. 112–126. DOI: https://doi.org/10.1016/j.seppur.2017.10.060.

[40] Michal Žák et al. 'Single-step purification of raw biogas to biomethane quality by hollow fiber membranes without any pretreatment – An innovation in biogas upgrading'. In: *Separation and Purification Technology* 203 (2018), pp. 36–40. DOI: https://doi.org/10.1016/j.seppur.2018.04.024.

[41] E. Chabanon et al. 'Study of an innovative gas-liquid contactor for CO2 absorption'. In: *Energy Procedia* 4 (2011), pp. 1769–1776. DOI: https://doi.org/10.1016/j.egypro.2011.02.052.

[42] Ingo Pinnau and Lora G. Toy. 'Gas and vapor transport properties of amorphous perfluorinated copolymer membranes based on 2,2-bistrifluoromethyl-4,5-difluoro-1,3-dioxole/tetrafluoroethylene'. In: *Journal of Membrane Science* 109.1 (1996), pp. 125–133. DOI: https://doi.org/10.1016/0376-7388(95)00193-X.